Global Field Time-Frequency Representation-Based Discriminative Similarity Analysis of Passive Auditory ERPs for Diagnosis of Disorders of Consciousness

Xiaoyu Wang, Yi Yang, Geoffrey Laforge, Xueling Chen, Loretta Norton, Adrian M. Owen, Jianghong He, and Fengyu Cong

***Abstract*— Behavioural diagnosis of patients with disorders of consciousness (DOC) is challenging and prone to inaccuracies. Consequently, there have been increased efforts to develop bedside assessment based on EEG and event-related potentials (ERPs) that are more sensitive to the neural factors supporting conscious awareness. However, individual detection of residual consciousness using these techniques is less established. Here, we hypothesize that the cross-state similarity (defined as the similarity between healthy and impaired conscious states) of passive brain responses to auditory stimuli can index the level of awareness in individual DOC patients. To this end, we introduce the global field time-frequency representation-based discriminative similarity analysis (GFTFR-DSA). This method quantifies the average cross-state similarity index between an individual patient and our constructed healthy templates using the GFTFR as an EEG feature. We demonstrate that the proposed GFTFR feature exhibits superior within-group consistency in 34 healthy controls over traditional EEG features such as temporal waveforms. Second, we observed the GFTFR-based similarity index was significantly higher in patients with a minimally conscious state (MCS, 40 patients) than those with unresponsive wakefulness syndrome (UWS, 54 patients), supporting our hypothesis. Finally, applying a linear support vector machine classifier for individual MCS/UWS classification, the model achieved a balanced accuracy and F1 score of 0.77. Overall, our findings indicate that combining discriminative and interpretable markers, along with automatic machine learning algorithms, is effective for the differential diagnosis in patients with DOC. Importantly, this approach can, in principle, be transferred into any ERP of interest to better inform DOC diagnoses.**

***Index Terms*— disorders of consciousness, EEG/ERPs, global field time-frequency representation, mismatch negativity, machine learning.**

This work was supported by National Natural Science Foundation of China (Grant No. 91748105 & 81600919), National Foundation in China (No. JCKY2019110B009 & 2020-JCJQ-JJ-252), Fundamental Research Funds for the Central Universities in Dalian University of Technology in China [DUT20LAB303 & DUT20LAB308], and Beijing Nova Program (Z181100006218050). The first two authors contributed equally to this work. Corresponding author: Jianghong He and Fengyu Cong.

Xiaoyu Wang and Fengyu Cong are with School of Biomedical Engineering, Faculty of Medicine, Dalian University of Technology, Dalian, 116024, China (email: cong@dlut.edu.cn)

Fengyu Cong is also with the Faculty of Information Technology, University of Jyväskylä, Jyväskylä, 40014, Finland, the School of Artificial Intelligence, Faculty of Electronic Information and Electrical Engineering, and the Key Laboratory of Integrated Circuit and Biomedical Electronic System, Dalian University of Technology, Dalian, 116024, China.

Yi Yang, Xueling Chen, and Jianghong He are with the Department of Neurosurgery, Beijing Tiantan Hospital, Capital Medical University, Beijing, 100700, China (email: he_jianghong@sina.cn).

Xiaoyu Wang, Geoffrey Laforge, Loretta Norton, and Adrian M. Owen are with the Western Institute of Neuroscience, Department of Physiology and Pharmacology, and Department of Psychology, Western University, London ON N6A 5B7, Canada.

I. Introduction

DISORDERS of consciousness (DOC) are a class of severe neurological conditions that include coma, the vegetative state (VS)—also known as unresponsive wakefulness syndrome (UWS)—and the minimally conscious state (MCS). DOC are primarily caused by traumatic brain injury, and vascular/anoxic etiologies [1], [2]. Patients with UWS have regular, or semi-regular, sleep and wake cycles (eyes open; high arousal) but, nevertheless, show no signs of awareness of themselves or the surrounding environment [3], [4]. Patients in a MCS, on the other hand, produce minimal but inconsistent behavioral evidence of awareness [5]. Accurately differentiating between different levels of awareness is crucial for guiding treatment and predicting prognosis for DOC patients [6]. Currently, the Coma Recovery Scale-Revised (CRS-R) is considered the gold standard for diagnosing DOC patients. The CRS-R consists of six hierarchical subscales designed to assess behavioral responses to external stimuli, including auditory, visual, motor, and oromotor function, as well as communication ability and level of arousal [7]. However, due to fluctuations in patients' level of arousal, or examiners' proficiency with the CRS-R, the estimated rate of misdiagnosis among DOC patients approaches 40%, especially if patients are not regularly assessed [8], [9]. These issues have prompted researchers to move beyond standardized behavioural measures and incorporate neurophysiological techniques, such as electroencephalography (EEG) and functional magnetic resonance imaging (fMRI), into the assessment protocol [10], [11].

Compared to fMRI, EEG is low-cost, portable, and easy to apply at a patient's bedside, making it ideally suited for DOC patients [12]–[14]. Early investigations into EEG biomarkers of awareness focused on the spectral characteristics of resting-state EEG. These biomarkers were gradually summarized as the 'ABCD' model, which organizes changes in EEG power spectra into four categories, reflecting the severity of thalamocortical deafferentation (detailed in [15], [16]). Later studies proposed new measures that capture different

aspects of EEG activity, such as functional connectivity (e.g., weighted symbolic mutual information; [17]) and information-sharing properties (e.g., permutation entropy and Kolmogorov complexity; [18], [19]). These measures have been shown to improve objective discrimination between MCS and UWS patients compared to previous techniques. Despite the significant strides in developing novel quantitative indices of awareness, resting-state paradigms can only assess spontaneous EEG activity; they cannot capture neural responses to external stimulation. Consequently, event-related potentials (ERPs), which quantify the EEG responses induced by sensory, cognitive, or motor stimuli, may provide powerful alternatives to resting-state EEG in the assessment of DOC patients [20].

One event-related approach, the auditory oddball paradigm, has been used extensively to assess the residual neural function of DOC patients. Auditory oddball tasks are designed to passively elicit discriminative neural responses to a repeated sound (standard) and a rare sound (deviant) [21]. In this context, these paradigms mainly evaluate: (1) primary sensory processing in the auditory cortex, indexed by the N1 component [22]; and (2) automatic deviance-detection based on sensory memory, indexed by the mismatch negativity response (MMN) [23]. Early research demonstrated that the absence of N1 and MMN components predicted non-awakening in coma patients with a specificity of 90.9%, commonly preceding conditions like UWS or worse [21], [24], thereby characterizing these deficits as indicators of UWS. In contrast, 73.7% of patients who regained consciousness, typically improving to MCS or better, exhibited the N1 component, while MMN was detected with a sensitivity of 30%, indicating an association of N1 with MCS diagnosis. These findings have informed the application of passive auditory ERPs in the diagnosis of chronic DOC. For example, Kotchoubey *et al.* reported that N1 was more frequently evoked in MCS than UWS patients, suggesting that MCS patients may have better-preserved sensory processing functions than UWS patients [25]. In addition, Boly *et al.* found that the backward connectivity from frontal to temporal cortex, which is involved in generating the MMN, was significantly impaired in UWS patients relative to MCS patients [26]. Furthermore, Faugeras *et al.* reported that MCS patients exhibited significantly larger MMN amplitudes than UWS patients [27]. In contrast, however, Sitt *et al.* reported that the topographical pattern of MMN did not differentiate UWS from MCS patients [28]. These group level inconsistencies may be due to the difficulties in using conventional participant-averaged measures (e.g., amplitude and latency) to evaluate ERP responses across patients with DOC.

Recently, researchers have investigated the use of machine learning algorithms to automatically quantify neural discriminability (e.g., between standard versus deviant stimuli) using multi-channel EEG waveforms from individual patients [29]–[31]. The fundamental hypothesis is that residual auditory discrimination, indexed by classification scores of EEG responses to standard or deviant sounds, corresponds to regained or preserved cognitive functions and/or level of awareness. For instance, Tzovara *et al.* developed a topography-based decoding algorithm and found that the progression of decoding accuracy (standard versus deviant) during acute coma predicted individual patient outcomes [30], [32]. Furthermore, King *et al.* introduced a time-resolved decoding approach to detect EEG responses to stimulus novelty, as elicited by the Local–Global paradigm (see [33] for task description) [29]. For local patterns indexed by MMN, the decoding performance did not differ significantly between UWS/MCS patients. In contrast, P3b responses elicited by higher-order global stimulus features were found to potentially indicate the state of awareness. Overall, patient-specific machine learning approaches that train and test decoding models using passive ERP data from the same patient may have limited diagnostic capacity in distinguishing UWS from MCS, despite showing high predictive performance in comatose patients.

To date, most studies have underutilized the neural responses derived from healthy controls (HCs), which have generally been employed as statistical reference levels for identifying specific functional deficits in DOC patients [17], [26], [34]. To address this issue, Armanfard *et al.* proposed a two-phase machine learning framework for identifying the MMN component [35]. This approach trained discriminative sub-spaces to classify neural responses to standard and deviant tones solely using EEG data from HCs. In patients, the trained sub-spaces were used to calculate the similarity of ERP responses between individual patients and HCs. Their method successfully predicted the recovery of awareness for two comatose patients, suggesting that the similarity-based analysis approach may be effective when transferred to DOC diagnoses. However, no direct single-participant model has been developed until now.

This study aimed to investigate whether the similarity of neural responses between DOC patients and HCs could differentiate UWS and MCS diagnoses among individual patients during a passive auditory processing task. To accomplish this, we developed the global field time-frequency representation-based discriminative similarity analysis (GFTFR-DSA). First, four types of candidate features were compared to capture consistent cross-participant brain patterns elicited by the mismatch paradigm. The proposed GFTFR feature showed the highest within-group consistency in 34 HCs and was used to construct healthy templates. Then, we investigated the discriminative capacity of cross-state (between DOC patients and HCs) GFTFR-based similarity in differentiating UWS (N = 54 patients) from MCS (N = 40 patients) diagnoses using group-level statistics. Finally, we demonstrated that incorporating a linear support vector machine (SVM) classifier with the discriminative similarity indices shows great potential for clinical applications.

II. DATA DESCRIPTION

A. Participants and EEG Data Acquisition

1) DOC Patients: One hundred patients with chronic DOC (28+ days since injury) were recruited from the Department of Neurosurgery, Seventh Medical Center of Chinese PLA General Hospital, between January 2017 and December 2018. Experienced neurologists assessed each patient using the CRS-R scale [7]. Inclusion criteria for this study included: patients diagnosed as UWS or MCS according to the CRS-R

TABLE I
INFORMATION ABOUT PARTICIPANTS

Group	Number of participants	Age (mean±SD)	Time since brain injury (mo)	CRS-R Score (mean±SD)	Etiology			Gender (M+F)
					Vascular	Traumatic	Anoxic	
HC	34	27.38 ± 2.54						20+18
MCS	40	46.38 ± 14.61	5.65 ± 4.75	11.43 ± 4.23	18	12	10	25+15
UWS	54	44.33 ± 16.91	5.40 ± 4.00	5.72 ± 1.56	16	20	18	34+20

UWS: unresponsive wakefulness syndrome, MCS: minimally conscious state, HC: healthy control, M: male, F: female, mo: month.

scores, who were in stable conditions, and free from skull deformations. Scalp EEG data was recorded at the patient's bedside using a 21-channel Nicolet recording device (Natus Neurology Inc.) according to the 10/20 International System. The sampling rate was 1000 Hz, and the impedances of the electrodes were kept below 10 kΩ. Data were referenced online at the CPz electrode. After visual inspection of raw EEG data, six patients were withdrawn due to high levels of non-physiological noise artifacts. Thus, 54 UWS and 40 MCS patients were retained for further analysis. The relevant demographics and clinical characteristics are summarized in Table I. This study was approved by the Ethics Commission of the Seventh Medical Center of Chinese PLA General Hospital, and written informed consents were acquired from all the patients' families and caregivers.

2) Healthy Controls: Thirty-eight normal-hearing healthy volunteers participated in the passive auditory ERPs experiment conducted in a sound-attenuated room. None had a history of neurological or psychiatric illnesses. Participants were instructed to sit relaxed on their chair and watch the movie *Modern Times* by Charlie Chaplin, with the sound muted. This task was chosen to keep the participants' attention from wandering, while requiring minimal effort. No behavioral response was required during the task. We collected EEG data with a 64-channel ANT recording device (ANT Neuro, Enschede) according to the 10/20 International System. We then reduced the number of electrodes offline to the same 21 channels as used in the DOC group. The sampling rate was 1000 Hz, and the impedances of the electrodes were kept below 10 kΩ. Data were referenced online at the CPz electrode. Following visual inspection of raw EEG data, four HCs were excluded due to high levels excessive motion artifacts (detailed in Table I) . This study was approved by the Ethics Commission of Dalian University of Technology. All participants gave written informed consent after the nature of the study was explained to them.

TABLE II
THE ACCEPTED NUMBER OF EPOCHS FOR EACH STIMULUS CONDITION

Group	1000 Hz epochs (Mean±SD)	1200 Hz deviant-minus-standard epochs	1050 Hz deviant-minus-standard epochs
HC	792 ± 11	99 ± 2	99 ± 2
MCS	748 ± 97	92 ± 14	93 ± 14
UWS	737 ± 92	90 ± 15	91 ± 14

UWS: unresponsive wakefulness syndrome, MCS: minimally conscious state, HC: healthy control.

B. Passive Auditory ERPs Paradigm

The current study used an auditory oddball paradigm consisting of two frequency deviation magnitudes to elicit N1 and MMN, as described in our previous studies [36], [37]. The standard tones were 1000 Hz and pure sounds at 1050 Hz and 1200 Hz served as the small and large deviants. All pure sounds were 200 ms in duration. The paradigm consisted of 1000 sound stimuli, which are uninterrupted and pseudo-randomly presented with the probability of 80%, 10%, and 10% for standard, small, and large deviant stimuli, respectively. A minimum of three standard stimuli preceded each deviant. The stimulus onset asynchrony was 1000 ms, and the experiment lasted approximately 1000 seconds in total. The stimulus sequence was programed in the Psychophysics Toolbox Version 3 [38] and delivered through headphones.

C. EEG Data Processing

1) Preprocessing: Preprocessing was conducted on continuous EEG data using MATLAB and the EEGLAB toolbox [39]. First, EEG data were visually inspected to remove significant artifacts caused by body movements, amplifier clipping, or bursts of EEG activity. Channels with excessive artifacts were interpolated using the spherical spline method. Continuous EEG data were down-sampled to 250 Hz. Basic filters embedded in EEGLAB were applied in the following order: 50 Hz notch filter, 1 Hz high-pass filter, and 30 Hz low-pass filter. The data were then re-referenced offline to the mean potential of two mastoid sites. Independent Component Analysis (ICA) was performed on filtered data using the InfomaxICA algorithm [40], specifically to remove eye blink and horizontal eye movement artifacts. We began by reducing the number of components to 15. Subsequently, the ICLabel toolbox [41] was used for automatic artifact identification, with each detected artifact then manually verified. Overall, ocular artifacts were identified and removed from 34/34 HCs, 25/40 patients with MCS, and 24/50 patients with UWS.

2) Extracting Epochs, Calculating the Difference Waves and Averaging: The preprocessed EEG data were segmented into 500 ms epochs, time-locked to stimulus onset, and included a pre-stimulus period of 100 ms (baseline). We then subtracted the baseline from each trial to ensure that all segments had the same origin. To isolate MMN component, we subtracted the preceding standard response from each deviant response to construct a set of single-trial difference waveforms. Trials with amplitude exceeding 100 μV were excluded. Table II shows the accepted number of epochs for each stimulus condition. We

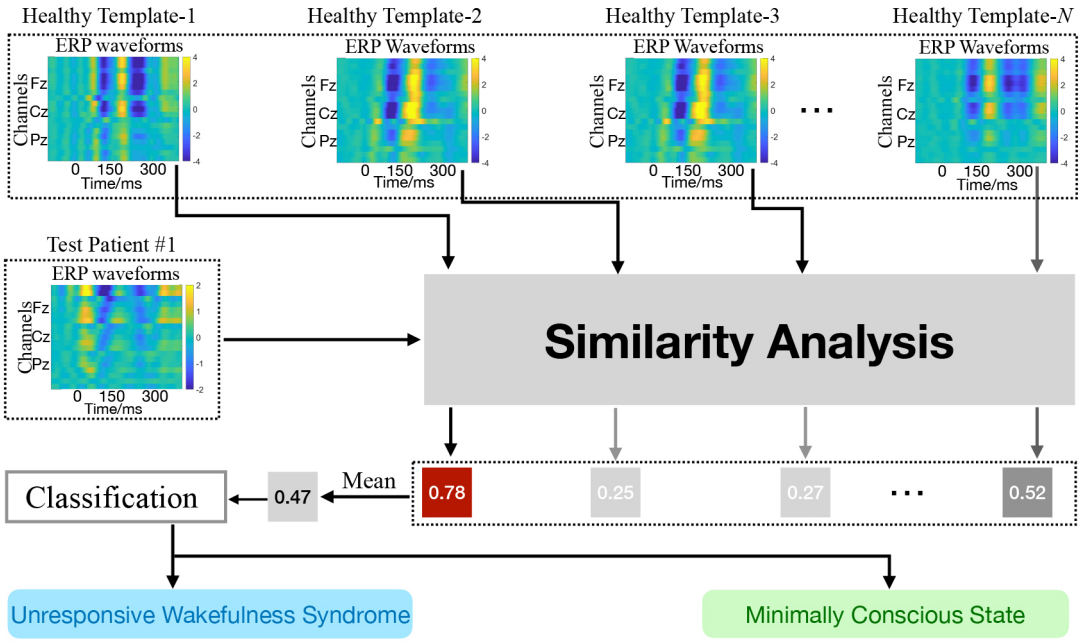

Fig. 1. Framework of the proposed discriminative similarity analysis.

calculated participant-averaged waveforms across the trials for three stimulus conditions at each channel. In total, there were three types of participant-averaged data for each participant: (a) PA_{1000} denotes the participant-averaged waveforms across all standard (1000 Hz) stimuli whereas (b) PA_{1200} and (c) PA_{1050} denote the averaged difference waveforms of 1200 Hz and 1050 Hz conditions, respectively.

III. Proposed Discriminative Similarity Analysis

Fig.1 shows an overview of the proposed framework for DOC diagnosis (constructing healthy templates using multi-channel temporal waveform as a feature). This includes the following steps: (1) extracting a list of candidate features from participant-averaged waveforms; (2) constructing healthy templates based on the candidate feature that achieves the highest within-group consistency; (3) calculating the cross-state similarity index (SI) of passive auditory brain responses between each DOC patient and HCs using the selected feature; and (4) passing the SIs into a linear SVM classifier to investigate MCS/UWS binary classification performance.

A. Cross-Participant Similarity Index (SI)

We used Pearson's linear correlation to quantify the cross-participant similarity of passive auditory brain responses. Here, $A \in \mathbb{R}^{C\times T}$ and, $B \in \mathbb{R}^{C\times T}$ are the 2-dimensional candidate features (e.g., temporal waveforms with C channels and T time-points) extracted from two participants. The SI can then be calculated as follows [42]:

$$\mathrm{SI}(A,B) = \frac{\sum_{c=1}^{C}\sum_{t=1}^{T}(A_{c,t}-\overline{A})(B_{c,t}-\overline{B})}{\sqrt{(\sum_{c=1}^{C}\sum_{t=1}^{T}(A_{c,t}-\overline{A})^2)(\sum_{c=1}^{C}\sum_{t=1}^{T}(B_{c,t}-\overline{B})^2)}} \quad (1)$$

where c denotes the channel number, $c = 1,\ldots,C$, t denotes a time-point, $t = 1,\ldots,T$, $\overline{A}$ and $\overline{B}$ denote the mean value of the corresponding matrix. As shown in Fig.1, we consider the candidate features extracted from HCs as normative templates, marked as $Temp \in \mathbb{R}^{C\times T}$. Then, the average ERP-based SI between a test participant (denoted as $A \in \mathbb{R}^{C\times T}$) and aggregate healthy templates can be calculated as follows:

$$\mathrm{SI}\_avg(A) = \frac{\sum_{m=1}^{M}\mathrm{SI}(A,Temp^m)}{M} \quad (2)$$

where $m = 1,\ldots,M$. M denotes the number of healthy templates and $Temp^m$ is the mth HC's feature template.

B. Candidate Features

In the framework, DOC classification performance depends on extracting informative and representational EEG features. Here, we compared four types of multi-dimensional features computed from participant-averaged waveforms, corresponding to three stimulus conditions.

1) Multi-channel Temporal Waveform (MTW): Initially, we used the MTW as the first candidate feature. Considering the three stimulus conditions in the current paradigm, three types of MTW were obtained for each participant: $PA_{1000}\mathbb{R}^{19\times125}$, $PA_{1200}\mathbb{R}^{19\times125}$ and $PA_{1050}\mathbb{R}^{19\times125}$ (19 channels × 125 time-points). Then, the MTW-based SI was computed via (1), and (2) for each condition, respectively.

2) Global Field Power (GFP): In terms of spatial activation patterns, ERPs are generated by synchronous brain activity at specific electrodes. GFP is a measure that characterizes the global activation pattern and is defined as the time series of the standard deviation across all electrodes [43]. For a given spatial map at the tth time-point, $A_{:,t} \in \mathbb{R}^{C\times1}$, the GFP amplitude can be computed as:

$$\mathrm{GFP}(A_{:,t}) = \sqrt{\frac{\sum_{c=1}^{C}(A_{c,t}-\overline{A_{:,t}})^2}{C}} \quad (3)$$

where $\overline{A_{:,t}}$ is the mean value over the C electrodes at the tth time-point. Then, for a given stimulus condition of MTW, e.g., $PA_{1000}\mathbb{R}^{19\times125}$, we can obtain GFP $(PA_{1000}) \in \mathbb{R}^{1\times125}$.

3) Time-Frequency Representation (TFR): To further explore the time-varying oscillatory properties of EEG time series, TFR shows promise for detecting and analyzing N1 and MMN components [44], [45]. Here, we adopted a continuous wavelet transform (CWT) to compute the TFR. For a given discrete time series of length-T at the cth channel, $A_{c,:} \in \mathbb{R}^{1\times T}$, the CWT is expressed as follows [46]:

$$\mathrm{CWT}(A_{c,:}) = \frac{1}{\sqrt{|a|}}\sum_{t=1}^{T} A_{c,t}\psi(\frac{t-b}{a}) \tag{4}$$

where t denotes a time-point, $t = 1,\ldots,T$, a and b are the scales and time shifting parameters, respectively. $\psi(t)$ is the mother wavelet, and $\psi(\frac{t-b}{a})$ is the shifted and scaled wavelet. We selected the complex Morlet wavelets as the 'mother' wavelet, which defined as [47]:

$$\psi(t) = \frac{1}{\sqrt{\pi\sigma^2}} e^{2\pi i f_c t} e^{-\frac{t^2}{2\sigma^2}} \tag{5}$$

where σ and f_c are frequency bandwidth and central frequency, respectively. We calculated TFRs for each condition from 1 to 10 Hz in 0.5 Hz steps by applying a CWT on each EEG channel using the '*cmor1-1.5*' function in MATLAB. Baseline subtraction was conducted with a -100 to 0 ms period.

For a given discrete time series at the cth channel (the green solid line in Fig.2a), $A_{c,:} \in \mathbb{R}^{1\times T}$, we can obtain $\mathrm{CWT}(A_{c,:}) \in \mathbb{R}^{T\times F}$ using equation (4) and (5), where T and F denote the number of time-point and frequency-point, respectively. Then, corresponding power (the time-frequency plot in Fig.2a) and phase can be computed as:

$$\mathrm{Power}(A_{c,:}) = \frac{\mathrm{CWT}(A_{c,:})^2}{F} \tag{6}$$

$$\mathrm{Phase}(A_{c,:}) = \arctan(\frac{\mathrm{Im}(\mathrm{CWT}(A_{c,:}))}{\mathrm{Re}(\mathrm{CWT}(A_{c,:}))}) \tag{7}$$

where $\arctan(\cdot)$ denotes the inverse tangent function, $\mathrm{Re}(\cdot)$ and $\mathrm{Im}(\cdot)$ denote the the real and imaginary part of a complex number. As shown in Fig.2b, for the given MTW, $A \in \mathbb{R}^{C\times T}$, the corresponding wavelet transform can be defined as:

$$\mathrm{CWT}(A) = [(\mathrm{Vec}(\mathrm{CWT}(A_{1,:}))\ldots\mathrm{Vec}(\mathrm{CWT}(A_{C,:}))]^T \tag{8}$$

where $\mathrm{Vec}(\cdot)$ denotes the matrix-to-vector conversion by concatenation of columns, the superscript T denotes the transpose, and $\mathrm{CWT}(A) \in \mathbb{R}^{C\times TF}$. Finally, as for the single-participant TFR features, we simultaneously considered the power and phase characteristics derived from the wavelet transform to measure the cross-participant similarity of ERP responses. Let $A \in \mathbb{R}^{C\times T}$ and $B \in \mathbb{R}^{C\times T}$ are the 2-dimensional MTW extracted from two participants, then, the TFR-based cross-participant SI can be computed as:

$$\begin{aligned}\mathrm{SI}(\mathrm{CWT}(A),\mathrm{CWT}(B)) = \mathrm{Sign}(\mathrm{SI}(\mathrm{Phase}(A),\mathrm{Phase}(B)))\\ \cdot \mathrm{SI}(\mathrm{Power}(A),\mathrm{Power}(B))\end{aligned} \tag{9}$$

where $\mathrm{sign}(\cdot)$ denotes the sign function.

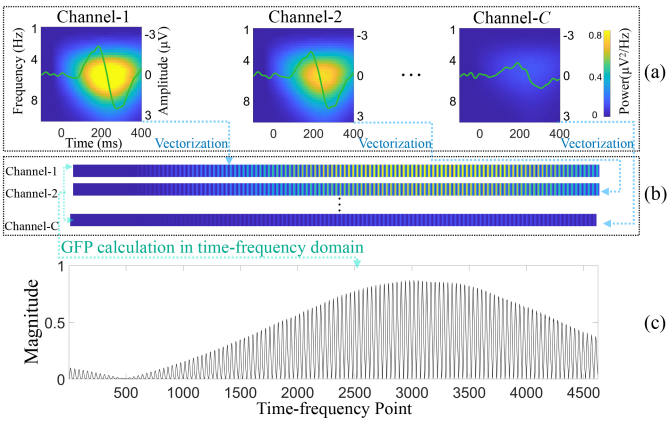

Fig. 2. Flowchart of calculating global field time-frequency representation. (a) single-channel temporal waveform (green solid line) and its time-frequency representation; (b) vectorization of single-channel time-frequency power; (c) global field time-frequency representation.

4) Global Field Time-Frequency Representation (GFTFR): To characterize the global activation patterns of time-varying oscillatory time series, we extended the temporal GFP measure to the time-frequency domain and proposed the novel GFTFR feature. For a given power-based spatial map at the nth time-frequency point, $\mathrm{Power}(A_{:,n})$, $n = 1,\ldots,TF$, T and F denote the number of time-point and frequency-point, as shown in Fig.2c, the GFTFR amplitude is defined as:

$$\mathrm{GFP}(\mathrm{Power}(A_{:,n})) = \sqrt{\frac{\sum_{c=1}^{C}(\mathrm{Power}(A_{c,n}) - \overline{\mathrm{Power}(A_{:,n})})^2}{C}} \tag{10}$$

where c denotes the channel number, $c = 1,\ldots,C$, and $\overline{\mathrm{Power}(A_{:,n})}$ denotes the mean power across all electrodes at the nth time-frequency point. Like (9), the GFTFR-based cross-participant SI can be computed as:

$$\begin{aligned}\mathrm{SI}(\mathrm{GTFFP}(A),\mathrm{GTFFP}(B)) = \mathrm{Sign}(\mathrm{SI}(\mathrm{Phase}(A),\mathrm{Phase}(B)))\\ \cdot \mathrm{SI}(\mathrm{GFP}(\mathrm{Power}(A)),\mathrm{GFP}(\mathrm{Power}(B)))\end{aligned} \tag{11}$$

where $A \in \mathbb{R}^{C\times T}$ and $B \in \mathbb{R}^{C\times T}$ are the 2-dimensional MTW extracted from two participants.

C. Statistical Analysis

1) Group-Level Analysis of ERPs Characteristics: First, one-tailed t-tests were computed to determine whether the N1 and MMN amplitudes significantly differed from zero, to first establish the existence of N1 and MMN components. To control for the use of different EEG devices, cross-group analysis was restricted to comparisons between MCS and UWS. Subsequently, we performed a one-way analysis of variance (ANOVA) to assess the impact of consciousness state on N1 and MMN amplitudes within these groups. We quantified the amplitudes at electrode Fz as: the mean value within a -5 to 5 ms time window centered on the most negative peak, occurring at 50-150 ms (N1) on the averaged parent waveforms elicited by all standard stimuli, and at 100-300 ms (MMN) on the difference waveforms (deviant minus standard).

2) Feature Selection via the Within-Group Consistency in HCs: Here, the goal is to construct healthy templates based on the candidate feature that achieved the highest within-group similarity consistency in HCs. We conducted a two-way repeated measures ANOVA to test the effects of feature types (four: MTW, GFP, TFR and GFTFR) and three stimulus conditions on the within-group SIs in HCs given by (2).

3) Discriminative Analysis of the Proposed SI in MCS and UWS Groups: After feature type determination, we computed an individual SI for each patient in the DOC cohort against a composite of healthy templates, as given by (2). To evaluate the discriminative capacity of the proposed measure, we aggregated the single-patient SI from all patients and performed a two-way repeated measures ANOVA to assess the effects of consciousness state (MCS and UWS) and three stimulus conditions. The statistical significance level was set at 0.05. Bonferroni corrections were applied to adjust for multiple comparisons regarding the main effect of stimulus conditions and the significant interaction effects. Statistical analyses were performed using IBM SPSS Statistics, Version 22.

D. Classification

1) Model and Cross-Validation: We used a linear SVM classifier [48] to investigate the extent to which the proposed single-patient SI could differentiate between MCS/UWS. The classification performance was evaluated using leave one participant out cross-validation. In this approach, one patient was selected for testing, while the remaining 93 patients were used for training the classifier. This process continued iteratively until all the participants were selected once, as the testing participant. Considering the imbalanced datasets, we employed sensitivity (SEN), specificity (SPE), balanced accuracy (B_ACC) and F1 score, to evaluate the classification performance, which can be computed as follows [49]:

$$SEN = TP/(TP + FN) \tag{12}$$

$$SPE = TN/(FP + TN) \tag{13}$$

$$B\_ACC = TP/(TP + FN) \tag{14}$$

$$F1 = 2 \times (SEN \times SPE)/(SEN + SPE) \tag{15}$$

where TP, TN, FP, and FN are the number of true positives, true negatives, false positives, and false negatives, respectively.

2) Comparison of Similarity Combination Strategies: As there were three types of participant-averaged data (PA_{1000}, PA_{1200}, and PA_{1050}), we obtained three paired SIs at individual level. Here, we employed B_ACC, SEN, SPE and F1 score, to investigate the optimal similarity combination in MCS/UWS classification. In total, there were seven options, including: three one-condition similarities, three two-condition similarity vectors and a three-condition similarity vector.

3) Comparison with Traditional Approach: As our approach was inspired by the method introduced by Armanfard *et al.* [35], we compared the individual-level classification performance of these two algorithms on the same dataset. The original method used a combination of feature extraction (FE) and localized feature selection (LFS) method (hereafter referred to as FE-LFS), and we applied the same techniques as suggested in original paper on our dataset [35]. The approach was performed in three steps: (1) training the FE-LFS model using data from HCs alone to classify between standard and deviant conditions; (2) calculating the single-patient similarity while testing the model with data from DOC patients; (3) adding the similarities into a SVM classifier to investigate MCS/UWS classification performance using the leave one participant out method. The classification performance was also evaluated by B_ACC, SEN, SPE and F1 score.

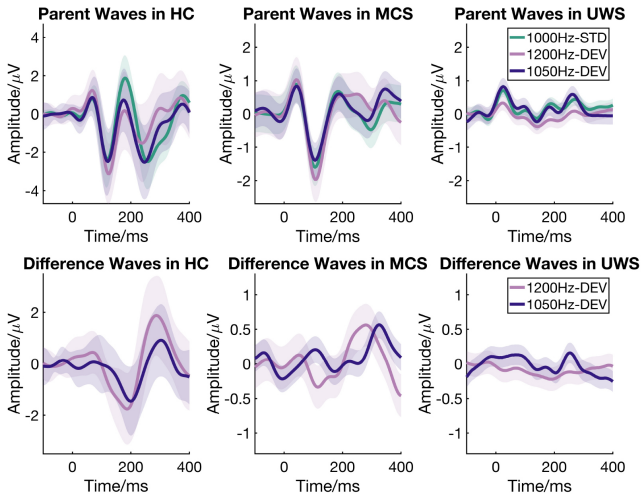

Fig. 3. Group-averaged waveforms at Fz electrode for different states of consciousness. Top panel represents the parent waves elicited by stimuli at frequencies of 1000Hz, 1200Hz, and 1050Hz, with shaded areas indicating the standard deviation among subjects. Bottom panels shows the difference waves, calculated by subtracting the EEG responses to standard stimuli from those to deviant stimuli under corresponding conditions. UWS: unresponsive wakefulness syndrome, MCS: minimally conscious state, HC: healthy control, STD: Standard, DEV: deviant.

IV. RESULTS

A. Group-Level Statistics of ERP Characteristics

Fig.3 presents group-averaged waveforms at Fz electrode across consciousness states. The top panel shows parent waves, demostrating the N1 component, and the bottom panel illustrates difference waves (deviant-minus-standard), revealing the MMN component. As shown in Table III, all N1 amplitudes differed significantly from zero in each group (all $t \leq -2.50$ and $p < 0.05$). A one-way ANOVA revealed that absolute N1 amplitudes significantly increased from UWS patients to MCS patients ($F = 11.63$, $p = 0.001$).

For the 1200 Hz deviant stimuli, MMN amplitudes were significantly different from zero in both HC and MCS groups (all $t \leq -2.04$ and $p < 0.05$). Conversely, in the UWS group, the MMN component was not significant ($t = -1.27$, $p = 0.21$). Further analysis using a one-way ANOVA indicated no notable difference in MMN amplitudes between the MCS and UWS groups ($p = 0.91$). Regarding the 1050 Hz deviant stimuli, the MMN was observed only in the HC group ($t = -6.97$, $p < 0.001$), with no significant components detected in either the MCS or UWS groups (all $t \geq -0.91$ and $p \geq 0.37$). A One-way ANOVA showed no significant differences between the MCS and UWS patients ($p = 0.49$).

TABLE III
THE MEAN ERP AMPLITUDES FOR THE THREE STIMULUS CONDITIONS IN THREE CONSCIOUSNESS STATES.

Group	N1 elicited by 1000 Hz stimuli		MMN elicited by 1200 Hz stimuli		MMN elicited by 1050 Hz stimuli	
	Mean ± SD	t	Mean ± SD	t	Mean ± SD	t
UWS	-0.29 ± 0.86	-2.50*	-0.20 ± 1.13	-1.27	-0.13 ± 1.03	-0.91
MCS	-1.11 ± 1.46	-4.82***	-0.32 ± 0.99	-2.04*	-0.10 ± 0.91	-0.70
HC	-2.40 ± 1.36	-10.30***	-1.87 ± 1.29	-8.46***	-1.59 ± 1.33	-6.97***

UWS: unresponsive wakefulness syndrome, MCS: minimally conscious state, HC: healthy control. Results of t-tests: $^{*}p < 0.05$, $^{***}p < 0.001$.

B. Within-Group Consistency of Candidate Features in HCs

To construct healthy EEG templates that capture consistent brain patterns across participants, we assessed the within-group consistency of all candidate features in HCs. Fig.4 presents the within-group consistency of candidate features in HCs among stimulus conditions (1000 Hz standards, 1200 Hz, and 1050 Hz deviants). Two-way (Feature × Condition) repeated measures ANOVA on the within-group similarity revealed a significantly interaction [$F = 35.34$, $p < 0.001$], as well as significant main effects of Feature [$F = 92.05$, $p < 0.001$] and Condition [$F = 240.05.63$, $p < 0.001$].

Simple effects analyses revealed that there were significant differences of individual SIs among feature types in the 1000 Hz, 1200 Hz and 1050 Hz conditions [1000 Hz: $F = 66.61$, $p < 0.001$; 1200 Hz: $F = 94.10$, $p < 0.001$; 1050 Hz: $F = 47.42$, $p < 0.001$]. As shown in the right panel of Fig.4, the GFTFR feature consistently achieved the highest within-group consistency among HCs across all conditions. Specifically, this was significant in the 1200 Hz condition (all $p < 0.05$). Moreover, no significant difference was observed between GFTFR and TFR at 1000 Hz (mean difference = 0.01), and similarly, there was no significant difference between GFP and GFTFR at 1050 Hz (mean difference = 0.05). For the Condition effect, within-group similarities in HCs significantly decreased (all $p < 0.05$) when moving from 1000 Hz standard stimuli to 1200 Hz, and to 1050 Hz deviant stimuli in all four types of candidate features [MTW: $F = 164.21$, $p < 0.001$; GFP: $F = 50.35$, $p < 0.001$; TFR: $F = 157.79$, $p < 0.001$; GFTFR: $F = 44.56$, $p < 0.001$]. Taken together, the GFTFR feature should be selected to construct healthy templates.

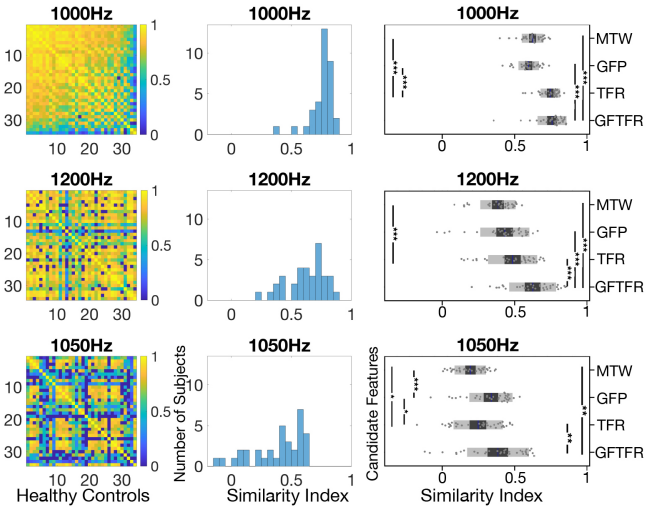

Fig. 4. Within-group consistency of candidate features in HCs under three stimulus conditions. Left panel: cross-participant similarity matrices of GFTFR feature; middle panel: histograms of individual similarity indices derived from the average GFTFR-based similarities between single participants and other HCs; right panel: statistical results of similarity index for candidate features. MTW: multi-channel temporal waveforms; GFP: global field power; TFR: time-frequency representation; GFTFR: global field time-frequency representation; HC: healthy control. * denotes $\boldsymbol{p < 0.05}$; ** denotes $\boldsymbol{p < 0.01}$; *** denotes $\boldsymbol{p < 0.001}$.

C. Cross-Group Discriminating Results of the GFTFR-based Cross-State SI

Fig.5 shows the cross-group discriminating results of the GFTFR-based similarity between MCS and UWS patients in three stimulus condition. Two-way (Group × Condition) repeated measures ANOVA on the single-patient SIs revealed a significant interaction effect [$F = 6.01$, $p < 0.01$], as well as significant main effects of Group [$F = 35.66$, $p < 0.001$] and Condition [$F = 19.89$, $p < 0.001$].

Simple effects analyses indicated that the cross-state SIs of MCS patients were significantly larger than those of UWS patients in 1000 Hz [$F = 19.31$, $p < 0.001$] and 1200 Hz [$F = 24.81$, $p < 0.001$] conditions, but not in 1050 Hz condition [$F = 3.36$, $p = 0.07$]. Additionally, a significant difference in similarity was found only in the Condition factor for MCS patients [$F = 26.10$, $p < 0.001$]. *Post hoc* analysis revealed that SIs in 1000 Hz condition were significantly larger than that of 1200 Hz and 1050 Hz conditions (all $p < 0.05$), whereas no such significant difference was found in the latter conditions ($p = 0.23$). Overall, the group-level statistics suggest that the GFTFR-based cross-state SI is a highly discriminative measure for UWS and MCS.

D. Individual MCS/UWS Classification Performance

Fig.6a illustrates the linearly separable distribution of the GFTFR-based SI at 1000 Hz and 1200 Hz, which significantly separates MCS from UWS. Consequently, we incorporated these discriminative SIs into a linear SVM classifier for MCS/UWS binary classification. Table IV shows the classification performance for different similarity combination strategies. Notably, the model achieved the highest performance, with balanced accuracy, sensitivity, specificity, and F1 score of 0.77, 0.73, 0.81, and 0.77, respectively, when using the three-condition similarity vectors as individual samples.

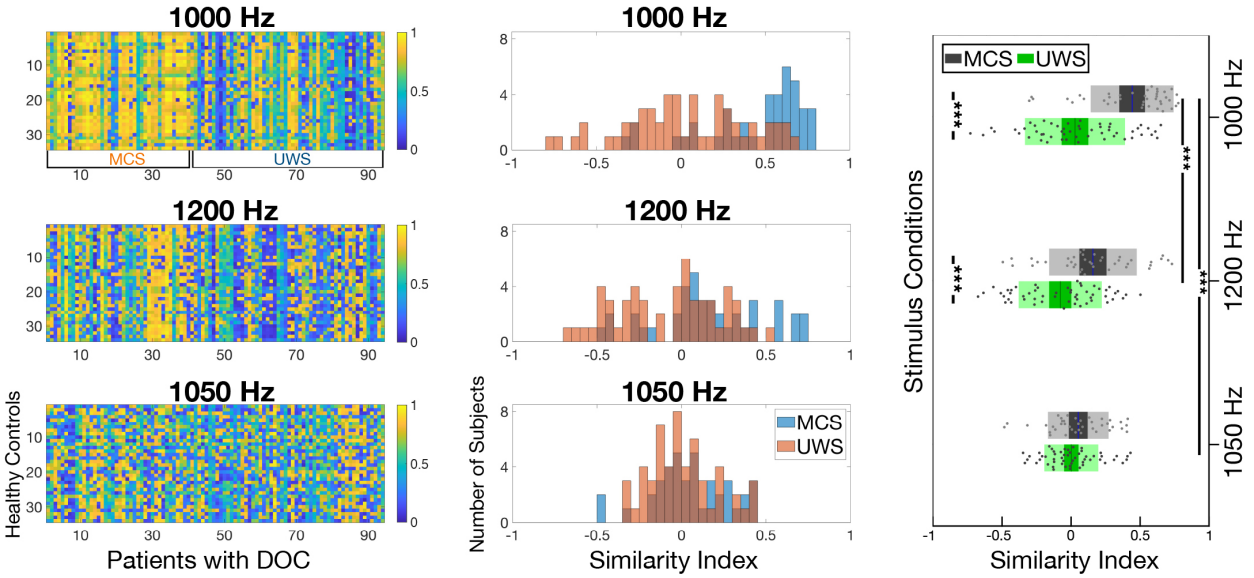

Fig. 5. Cross-group discriminating results of the GFTFR-based similarity between MCS and UWS patients in three stimulus conditions. Left panel: cross-state similarity matrices between patients with DOC and healthy templates; middle panel: histograms of individual patient similarity index, deriving from the average cross-state similarities between each DOC patient and all healthy templates; left panel: statistical results of GFTFR-based similarity index. GFTFR: global field time-frequency representation; DOC: disorders of consciousness; UWS: unresponsive wakefulness syndrome, MCS: minimally conscious state. * denotes $\boldsymbol{p < 0.05}$; ** denotes $\boldsymbol{p < 0.01}$; *** denotes $\boldsymbol{p < 0.001}$.

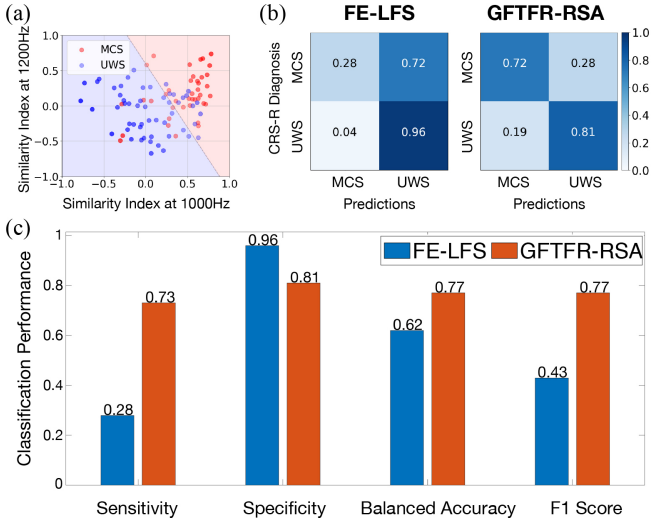

Fig. 6. (a) Linearly separable distribution of GFTFR-Based similarity index at 1000 Hz and 1200 Hz; (b) Confusion matrices for FE-LFS and GFTFR-DSA methods; (c) Classification performance indices for above methods. FE-LFS: feature extraction combines localized feature selection method proposed by Armanfard *et al.* [35]; GFTFR-DSA: global field time-frequency representation-based discriminative similarity analysis proposed in this study. UWS: unresponsive wakefulness syndrome, MCS: minimally conscious state.

Moreover, as for the comparison with the traditional approach, Fig.6b,c illustrates the confusion matrices and performance indices for FE-LFS and GFTFR-DSA methods. In short, our proposed approach achieved a much better MCS/UWS classification performance, with the F1 score increasing from 0.43 to 0.77.

E. Effects of Clinical Factors on Classification Accuracy

Finally, to evaluate the effects of clinical factors on diagnosis performance, we performed a one-way repeated measures ANOVA on diagnosis accuracy (true and false predictions were defined as 1 and 0) for three critical clinical factors (Etiology, Course of Disease, and Age). As shown in Fig.7, a significant difference was only observed in Age [$F = 3.89$, $p = 0.02$] but not in Etiology [$F = 0.29$, $p = 0.75$] or Course of Disease [$F = 0.16$, $p = 0.85$]. *Post hoc* analysis revealed that our method achieved significantly higher classification accuracies in patients ≤ 40 years than in patients between 40 and 55 years (mean $= 0.656$, $p = 0.021$) and ≥ 55 years (mean $= 0.742$, $p = 0.152$). No significant difference was observed in the latter two groups. Overall, the current results suggest that our technique is robust in the face of various clinical factors.

V. DISCUSSION

In this study, we introduced a novel approach that combines the GFTFR-based cross-state similarity and machine learning classifiers to assess the severity of chronic DOC. Overall, this study presents three novel techniques that complement conventionally methods of DOC assessment. To the best of our knowledge, we are the first to apply the GFTFR feature to characterize the temporal, spectral, and spatial signatures of dynamic EEG activity in this patient group. Among the four types of candidate features, GFTFR achieved the highest within-group similarity in HCs. Additionally, to capture the time-varying oscillatory properties of EEG, the proposed cross-participant SI simultaneously quantified the power and phase characteristics derived from the wavelet transform. Moreover, we sought to determine the level of awareness in individual DOC patients using GFTFR-based cross-state

TABLE IV
THE CLASSIFICATION PERFORMANCE FOR DIFFERENT SIMILARITY COMBINATION STRATEGIES

Index	1050 Hz	1200 Hz	1000 Hz	1050 Hz & 1200 Hz	1050 Hz & 1000 Hz	1200 Hz & 1000 Hz	1050 Hz & 1200 Hz & 1000 Hz
Sensitivity	0	0.38	0.73	0.35	0.70	0.73	0.73
Specificity	1	0.80	0.76	0.81	0.78	0.78	0.81
Balanced Accuracy	0.50	0.59	0.74	0.58	0.74	0.75	0.77
F1 Score	0	0.52	0.74	0.49	0.74	0.75	0.77

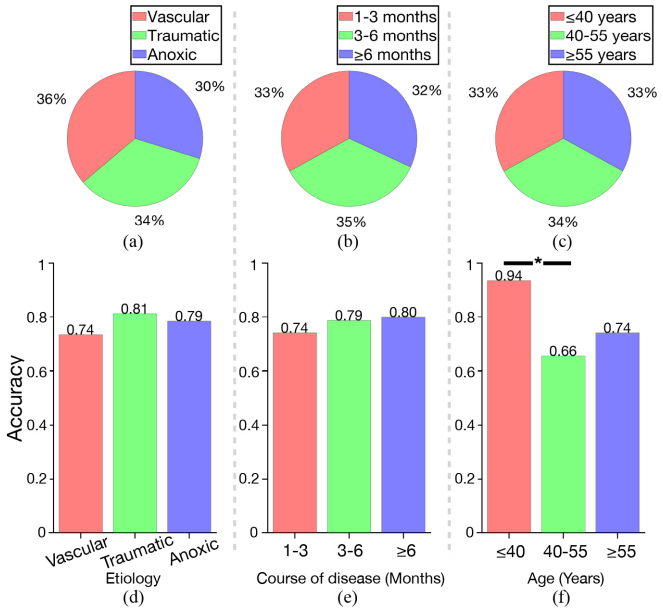

Fig. 7. Effects of three critical clinical factors on classification accuracy. The proportion of patients in (a) etiology (b) course of disease and (c) age factors; (d) - (f) represent the individual-level classification accuracy for the above clinical factors.

(between patients and HCs) SIs, which are readily interpretable and discriminative of conscious state.

A. GFTFR Uncovers the Consistent Characteristics of Passive Auditory ERPs in HCs

The mark of an effective DOC diagnosis is high within-group consistency (e.g., similar index strengths among HCs) and large cross-group differences (e.g., individuals diagnosed with various levels of severity demonstrate significantly different strengths). However, inherent individual variability of EEG/ERPs can critically affect the former [50]. Consequently, capturing the shared activation patterns among HCs using the appropriate features improves within-group consistency significantly. Our results indicated that the proposed GFTFR feature achieved significantly higher within-group similarities between HCs than the other candidate features. We speculate that two factors may account for these results. First, GFTFR is effective in capturing the frequency-specific properties of time-locked N1 and MMN components. Previous investigations reported that N1 and MMN components predominantly consist of activity in the theta band ($\approx$ 4–8 Hz). Researchers have also demonstrated the advantages of quantifying theta oscillations over the temporal measures [44], [51]. For example, Bishop and Hardiman were able to identify a theta-band phase-locking enhancement in 82% of their participants but this drops to 70% if the MMN was analyzed in the time domain [44]. The present study found that within-group similarities of time-frequency features were significantly higher than that of temporal waveforms, in line with the previous studies. Moreover, GFTFR might benefit from the dimension reduction process through calculating the standard deviations across channels. Compared to multi-channel waveforms, GFP can characterize the global activation pattern in a relatively low spatial dimension (i.e., the number of spatial dimensions reduced from the number of electrodes to 1; [43]). Taken together, these findings suggest that GFTFR can be useful when analyzing the cross-participant consistent characteristics of passive auditory ERPs.

Regarding the stimulus conditions, we found that the within-group SIs in HCs significantly decreased when moving from 1000 Hz standard stimuli to 1200 Hz deviant stimuli, and to 1050 Hz deviant stimuli in all candidate features. The differences of signal-to-noise-ratio (SNR) across conditions were supposed to explain the significant effect of stimulus conditions. The SNR increases in proportion to the square root of the number of trials [20]. Our paradigm consisted of 800 standards and 100 deviants (e.g., 1200 Hz deviant stimulus) and the present study extracted the candidate features on the averaged waveforms across trials for each condition. Consequently, the SNR of standard condition is 2.83 ($\sqrt{800}/\sqrt{100}$) times that of deviant condition, which determined the significant difference of within-group similarities between standard and deviant stimulus. In addition, an important property of MMN is that its amplitude (indexing the SNR) increases alongside the magnitude of sound change [52]. Our results confirmed that 1200 Hz deviants elicited larger MMN amplitudes (-1.87 $\pm$ 1.29 μV) than that of 1050 Hz deviants (-1.59 $\pm$ 1.33 μV), which led to the significant difference of within-group SI between two deviance magnitudes.

B. GFTFR-based Cross-State SI Provides Signature in UWS versus MCS Diagnosis

We hypothesized that the cross-state SI (between DOC patients and aggregate HCs) of passive auditory brain responses would correspond to conscious state. Our results showed that the proposed GFTFR-based cross-state SI of MCS patients were significantly higher than that of UWS patients, which supported our initial hypothesis. Our results are generally consistent with previous findings, as they demonstrated that

MCS patients showed cortical activation that was more similar to HCs, relative to UWS patients [17], [26], [34]. Notably, there were significant SI differences between MCS and UWS patients, whereas a significant cross-group difference was only observed in N1 amplitudes elicited by 1000 Hz standard stimuli. Our approach, therefore, has advantages in separating UWS from MCS over conventional ERPs analysis. Additionally, the proposed cross-state SI is easy to interpret, which may be advantageous in clinical settings.

Moreover, we demonstrated the use of machine learning for individual-level DOC diagnosis. Among various similarity combinations, the model achieved the best performance when using the three-condition similarity vectors to construct the input samples. This may indicate that N1 and MMN may provide complementary information in DOC assessment. In practice, several studies have suggested that this is the case, as they regarded the presence of N1 as a prerequisite for accurately measuring MMN [24], [34], emphasizing that using multiple EEG components derived from the same paradigm may improve the accuracy of DOC diagnosis and prognosis [14].Our study demonstrated the added value of combining N1 and MMN components to facilitate chronic DOC assessment. In summary, our findings demonstrate that the proposed GFTFR-based cross-state SI performs well when indexing conscious state, and enables the automatic diagnosis of individuals with machine learning techniques.

Notably, there are several limitations in the present study. First, in terms of training the MCS/UWS binary classifier, we derived the ground-truth using the CRS-R assessment, which may fail to accurately diagnose DOC patients. As a recent review suggested, this problem should be addressed in future studies by refining the diagnostic labels using additional multi-paradigm and multi-modality markers [15]. In addition, our healthy controls were younger overall and from a narrower age range than our patients with DOC. As there is evidence showing that the N1 and MMN characteristics change with age, the diagnostic performance of the proposed method could potentially be skewed [53]. Furthermore, in the patient population, MMN may exhibit waxing and waning patterns, leading to instances where it could go undetected after aggregate averaging [35], [54]. Our current study has not yet explored MMN detection on this finer temporal scale, which might result in MCS patients who do possess MMN being overlooked in such aggregate analyses, thereby affecting the overall diagnostic performance. Taken together, with refined diagnostic labels, age-related alterations, and analysis on a finer temporal scale, it is to be expected that further work will improve diagnostic performance in DOC even further.

VI. Conclusion

In conclusion, this study introduces a novel machine learning approach, known as GFTFR-DSA, for neurophysiology-based diagnosis of DOCs. The proposed GFTFR features effectively capture shared EEG characteristics in terms of within-group consistency among healthy controls. By quantifying the GFTFR-based similarity between healthy and impaired conscious states, we have demonstrated that cross-state similarity can index the level of awareness in DOC patients. Moreover, incorporating discriminative markers with automatic SVM classifiers, our method enhances differential diagnosis in individual-level MCS/UWS discrimination. Overall, this approach complements conventional methods of DOC assessment and can be extended to any ERP of interest to better inform DOC diagnoses.

Reference

[1] J. T. Giacino, D. I. Katz, N. D. Schiff, J. Whyte, E. J. Ashman, S. Ashwal, R. Barbano, F. M. Hammond, S. Laureys, G. S. Ling, R. Nakase-Richardson, R. T. Seel, S. Yablon, T. S. Getchius, G. S. Gronseth, and M. J. Armstrong, "Practice guideline update recommendations summary: Disorders of consciousness," *Neurology*, vol. 91, no. 10, pp. 450–460, 2018.

[2] D. Kondziella, A. Bender, K. Diserens, W. van Erp, A. Estraneo, R. Formisano, S. Laureys, L. Naccache, S. Ozturk, B. Rohaut, J. D. Sitt, J. Stender, M. Tiainen, A. O. Rossetti, O. Gosseries, C. Chatelle, and the EAN Panel on Coma, Disorders of Consciousness, "European Academy of Neurology guideline on the diagnosis of coma and other disorders of consciousness," *European Journal of Neurology*, vol. 27, no. 5, pp. 741–756, 2020.

[3] B. Jennett and F. Plum, "Persistent vegetative state after brain damage: A syndrome in search of a name," *The Lancet*, vol. 299, no. 7753, pp. 734–737, 1972.

[4] Multi-Society Task Force on PVS, "Medical aspects of the persistent vegetative state," *New England Journal of Medicine*, vol. 330, no. 21, pp. 1499–1508, 1994.

[5] J. T. Giacino, S. Ashwal, N. Childs, R. Cranford, B. Jennett, D. I. Katz, J. P. Kelly, J. H. Rosenberg, JOHN. Whyte, and R. D. Zafonte, "The minimally conscious state: Definition and diagnostic criteria," *Neurology*, vol. 58, no. 3, pp. 349–353, 2002.

[6] M. R. Coleman, M. H. Davis, J. M. Rodd, T. Robson, A. Ali, A. M. Owen, and J. D. Pickard, "Towards the routine use of brain imaging to aid the clinical diagnosis of disorders of consciousness," *Brain*, vol. 132, no. 9, pp. 2541–2552, 2009.

[7] J. T. Giacino, K. Kalmar, and J. Whyte, "The JFK Coma Recovery Scale-Revised: Measurement characteristics and diagnostic utility," *Archives of physical medicine and rehabilitation*, vol. 85, no. 12, pp. 2020–2029, 2004.

[8] C. Schnakers, A. Vanhaudenhuyse, J. Giacino, M. Ventura, M. Boly, S. Majerus, G. Moonen, and S. Laureys, "Diagnostic accuracy of the vegetative and minimally conscious state: Clinical consensus versus standardized neurobehavioral assessment," *BMC Neurology*, vol. 9, no. 1, p. 35, 2009.

[9] S. Wannez, L. Heine, M. Thonnard, O. Gosseries, S. Laureys, and Coma Science Group collaborators, "The repetition of behavioral assessments in diagnosis of disorders of consciousness: Repeated CRS-R Assessments for Diagnosis in DOC," *Annals of Neurology*, vol. 81, no. 6, pp. 883–889, 2017.

[10] D. Cruse, S. Chennu, C. Chatelle, T. A. Bekinschtein, D. Fernández-Espejo, J. D. Pickard, S. Laureys, and A. M. Owen, "Bedside detection of awareness in the vegetative state: A cohort study," *The Lancet*, vol. 378, no. 9809, pp. 2088–2094, 2011.

[11] A. M. Owen, M. R. Coleman, M. Boly, M. H. Davis, S. Laureys, and J. D. Pickard, "Detecting awareness in the vegetative state," *Science*, vol. 313, no. 5792, pp. 1402–1402, 2006.

[12] D. A. Engemann, F. Raimondo, J.-R. King, B. Rohaut, G. Louppe, F. Faugeras, J. Annen, H. Cassol, O. Gosseries, D. Fernandez-Slezak, S. Laureys, L. Naccache, S. Dehaene, and J. D. Sitt, "Robust EEG-based cross-site and cross-protocol classification of states of consciousness," *Brain*, vol. 141, no. 11, pp. 3179–3192, 2018.

[13] P. Gui, Y. Jiang, D. Zang, Z. Qi, J. Tan, H. Tanigawa, J. Jiang, Y. Wen, L. Xu, J. Zhao, Y. Mao, M.-m. Poo, N. Ding, S. Dehaene, X. Wu, and L. Wang, "Assessing the depth of language processing in patients with disorders of consciousness," *Nature Neuroscience*, vol. 23, no. 6, pp. 761–770, 2020.

[14] J. Pan, Q. Xie, P. Qin, Y. Chen, Y. He, H. Huang, F. Wang, X. Ni, A. Cichocki, R. Yu, and Y. Li, "Prognosis for patients with cognitive motor dissociation identified by brain-computer interface," *Brain*, vol. 143, no. 4, pp. 1177–1189, 2020.

[15] A. Comanducci, M. Boly, J. Claassen, M. De Lucia, R. Gibson, E. Juan, S. Laureys, L. Naccache, A. Owen, M. Rosanova, A. Rossetti, C. Schnakers, J. Sitt, N. Schiff, and M. Massimini, "Clinical and advanced neurophysiology in the prognostic and diagnostic evaluation of disorders of consciousness: Review of an IFCN-endorsed expert group," *Clinical Neurophysiology*, vol. 131, no. 11, pp. 2736–2765, 2020.

[16] B. L. Edlow, J. Claassen, N. D. Schiff, and D. M. Greer, "Recovery from disorders of consciousness: Mechanisms, prognosis and emerging therapies," *Nature Reviews Neurology*, vol. 17, no. 3, pp. 135–156, 2021.

[17] J.-R. King, J. D. Sitt, F. Faugeras, B. Rohaut, I. El Karoui, L. Cohen, L. Naccache, and S. Dehaene, "Information Sharing in the Brain Indexes Consciousness in Noncommunicative Patients," *Current Biology*, vol. 23, no. 19, pp. 1914–1919, 2013.

[18] C. Bandt and B. Pompe, "Permutation Entropy: A Natural Complexity Measure for Time Series," *Physical Review Letters*, vol. 88, no. 17, p. 174102, 2002.

[19] A. G. Casali, O. Gosseries, M. Rosanova, M. Boly, S. Sarasso, K. R. Casali, S. Casarotto, M.-A. Bruno, S. Laureys, G. Tononi, and M. Massimini, "A Theoretically Based Index of Consciousness Independent of Sensory Processing and Behavior," *Science Translational Medicine*, vol. 5, no. 198, pp. 198ra105–198ra105, 2013.

[20] S. J. Luck, *An Introduction to the Event-Related Potential Technique*. Cambridge, Massachusetts: The MIT Press, second edition ed., 2014.

[21] D. Morlet and C. Fischer, "MMN and Novelty P3 in Coma and Other Altered States of Consciousness: A Review," *Brain Topography*, vol. 27, no. 4, pp. 467–479, 2014.

[22] R. Näätänen and T. Picton, "The N1 wave of the human electric and magnetic response to sound: A review and an analysis of the component structure.," *Psychophysiology*, vol. 24 4, pp. 375–425, 1987.

[23] R. Näätänen, A. W. Gaillard, and S. Mäntysalo, "Early selective-attention effect on evoked potential reinterpreted," *Acta psychologica*, vol. 42, no. 4, pp. 313–329, 1978.

[24] C. Fischer, D. Morlet, P. Bouchet, J. Luaute, C. Jourdan, and F. Salord, "Mismatch negativity and late auditory evoked potentials in comatose patients," *Clinical Neurophysiology*, vol. 110, no. 9, pp. 1601–1610, 1999.

[25] B. Kotchoubey, S. Lang, G. Mezger, D. Schmalohr, M. Schneck, A. Semmler, V. Bostanov, and N. Birbaumer, "Information processing in severe disorders of consciousness: Vegetative state and minimally conscious state," *Clinical Neurophysiology*, vol. 116, no. 10, pp. 2441–2453, 2005.

[26] M. Boly, M. I. Garrido, O. Gosseries, M.-A. Bruno, P. Boveroux, C. Schnakers, M. Massimini, V. Litvak, S. Laureys, and K. Friston, "Preserved Feedforward But Impaired Top-Down Processes in the Vegetative State," *Science*, vol. 332, no. 6031, pp. 858–862, 2011.

[27] F. Faugeras, B. Rohaut, N. Weiss, T. Bekinschtein, D. Galanaud, L. Puybasset, F. Bolgert, C. Sergent, L. Cohen, S. Dehaene, and L. Naccache, "Event related potentials elicited by violations of auditory regularities in patients with impaired consciousness," *Neuropsychologia*, vol. 50, no. 3, pp. 403–418, 2012.

[28] J. D. Sitt, J.-R. King, I. El Karoui, B. Rohaut, F. Faugeras, A. Gramfort, L. Cohen, M. Sigman, S. Dehaene, and L. Naccache, "Large scale screening of neural signatures of consciousness in patients in a vegetative or minimally conscious state," *Brain*, vol. 137, no. 8, pp. 2258–2270, 2014.

[29] J. R. King, F. Faugeras, A. Gramfort, A. Schurger, I. E. Karoui, J. D. Sitt, B. Rohaut, C. Wacongne, E. Labyt, T. Bekinschtein, L. Cohen, L. Naccache, and S. Dehaene, "Single-trial decoding of auditory novelty responses facilitates the detection of residual consciousness," *NeuroImage*, vol. 83, pp. 726–738, 2013.

[30] A. Tzovara, A. O. Rossetti, L. Spierer, J. Grivel, M. M. Murray, M. Oddo, and M. De Lucia, "Progression of auditory discrimination based on neural decoding predicts awakening from coma," *Brain*, vol. 136, no. 1, pp. 81–89, 2013.

[31] A. Tzovara, A. O. Rossetti, E. Juan, T. Suys, D. Viceic, M. Rusca, M. Oddo, and M. D. Lucia, "Prediction of awakening from hypothermic postanoxic coma based on auditory discrimination: Awakening from Postanoxic Coma," *Annals of Neurology*, vol. 79, no. 5, pp. 748–757, 2016.

[32] A. Tzovara, M. M. Murray, G. Plomp, M. H. Herzog, C. M. Michel, and M. De Lucia, "Decoding stimulus-related information from single-trial EEG responses based on voltage topographies," *Pattern Recognition*, vol. 45, no. 6, pp. 2109–2122, 2012.

[33] T. A. Bekinschtein, S. Dehaene, B. Rohaut, F. Tadel, L. Cohen, and L. Naccache, "Neural signature of the conscious processing of auditory regularities," *Proceedings of the National Academy of Sciences*, vol. 106, no. 5, pp. 1672–1677, 2009.

[34] V. Wijnen, G. van Boxtel, H. Eilander, and B. de Gelder, "Mismatch negativity predicts recovery from the vegetative state," *Clinical Neurophysiology*, vol. 118, no. 3, pp. 597–605, 2007.

[35] N. Armanfard, M. Komeili, J. P. Reilly, and J. F. Connolly, "A Machine Learning Framework for Automatic and Continuous MMN Detection With Preliminary Results for Coma Outcome Prediction," *IEEE Journal of Biomedical and Health Informatics*, vol. 23, no. 4, pp. 1794–1804, 2019.

[36] X. Wang, R. Fu, X. Xia, X. Chen, H. Wu, N. Landi, K. Pugh, J. He, and F. Cong, "Spatial Properties of Mismatch Negativity in Patients with Disorders of Consciousness," *Neuroscience Bulletin*, vol. 34, no. 4, pp. 700–708, 2018.

[37] X. Wang, Y. Guo, Y. Zhang, J. Li, Z. Gao, Y. Li, T. Zhou, H. Zhang, J. He, and F. Cong, "Combined Behavioral and Mismatch Negativity Evidence for the Effects of Long-Lasting High-Definition tDCS in Disorders of Consciousness: A Pilot Study," *Frontiers in Neuroscience*, vol. 14, p. 381, 2020.

[38] D. H. Brainard, "The psychophysics toolbox," *Spatial vision*, vol. 10, no. 4, pp. 433–436, 1997.

[39] A. Delorme and S. Makeig, "EEGLAB: An open source toolbox for analysis of single-trial EEG dynamics including independent component analysis," *Journal of neuroscience methods*, vol. 134, no. 1, pp. 9–21, 2004.

[40] TW. Lee, M. Girolami, and TJ. Sejnowski, "Independent component analysis using an extended infomax algorithm for mixed subgaussian and supergaussian sources," *Neural computation*, vol. 11, no. 2, pp. 417—441, 1999.

[41] L. Pion-Tonachini, K. Kreutz-Delgado, and S. Makeig, "ICLabel: An automated electroencephalographic independent component classifier, dataset, and website," *NeuroImage*, vol. 198, pp. 181–197, 2019.

[42] M. M. Mukaka, "Statistics corner: A guide to appropriate use of correlation coefficient in medical research," *Malawi medical journal : the journal of Medical Association of Malawi*, vol. 24, no. 3, pp. 69–71, 2012.

[43] W. Skrandies, "Global field power and topographic similarity," *Brain topography*, vol. 3, no. 1, pp. 137–141, 1990.

[44] D. V. M. Bishop and M. J. Hardiman, "Measurement of mismatch negativity in individuals: A study using single-trial analysis," *Psychophysiology*, vol. 47, no. 4, pp. 697–705, 2010.

[45] LL. Fuentemilla, J. Marco-Pallarés, TF. Münte, and C. Grau, "Theta EEG oscillatory activity and auditory change detection," *Brain research*, vol. 1220, pp. 93–101, 2008.

[46] F. Cong, T. Ristaniemi, and H. Lyytinen, *Advanced Signal Processing on Brain Event-Related Potentials: Filtering ERPs in Time, Frequency and Space Domains Sequentially and Simultaneously*, vol. 13. World Scientific, 2015.

[47] A. Teolis and J. J. Benedetto, *Computational Signal Processing with Wavelets*, vol. 182. Springer, 1998.

[48] I. Steinwart and A. Christmann, *Support Vector Machines*. Springer Science & Business Media, 2008.

[49] K. H. Brodersen, C. S. Ong, K. E. Stephan, and J. M. Buhmann, "The Balanced Accuracy and Its Posterior Distribution," in *2010 20th International Conference on Pattern Recognition*, (Istanbul, Turkey), pp. 3121–3124, IEEE, 2010.

[50] E. Pekkonen, T. Rinne, and R. Näätänen, "Variability and replicability of the mismatch negativity," *Electroencephalography and Clinical Neurophysiology/Evoked Potentials Section*, vol. 96, no. 6, pp. 546–554, 1995.

[51] B. J. Roach, J. M. Ford, R. L. Loewy, B. K. Stuart, and D. H. Mathalon, "Theta Phase Synchrony Is Sensitive to Corollary Discharge Abnormalities in Early Illness Schizophrenia but Not in the Psychosis Risk Syndrome," *Schizophrenia Bulletin*, vol. 47, no. 2, pp. 415–423, 2021.

[52] S. Pakarinen, R. Takegata, T. Rinne, M. Huotilainen, and R. Näätänen, "Measurement of extensive auditory discrimination profiles using the mismatch negativity (MMN) of the auditory event-related potential (ERP)," *Clinical Neurophysiology*, vol. 118, no. 1, pp. 177–185, 2007.

[53] M. Aghamolaei, Z. Jafari, S. Grimm, K. Zarnowiec, M. Najafi-Koopaie, and C. Escera, "The effects of aging on early stages of the auditory deviance detection system," *Clinical Neurophysiology*, vol. 129, no. 11, pp. 2252–2258, 2018.

[54] A. Herrera-Diaz, R. Boshra, P. Tavakoli, C.-Y. A. Lin, N. Pajankar, E. Bagheri, R. Kolesar, A. Fox-Robichaud, C. Hamielec, J. P. Reilly, *et al.*, "Tracking auditory mismatch negativity responses during full conscious state and coma," *Frontiers in Neurology*, vol. 14, p. 1111691, 2023.